



Published in final edited form as:

J Inorg Biochem. 2022 May ; 230: 111774. doi:10.1016/j.jinorgbio.2022.111774.

Visualizing the gas channel of a monofunctional carbon monoxide dehydrogenase

Alison Biester^a, Sébastien Dementin^c, Catherine L. Drennan^{a,b,d,e,*}

^aDept. of Chemistry, Massachusetts Institute of Technology, Cambridge, MA 02139, United States

^bDept. of Biology, Massachusetts Institute of Technology, Cambridge, MA 02139, United States

^cCNRS, Aix-Marseille Université, Laboratoire de Bioénergétique et Ingénierie des Protéines, Institut de Microbiologie de la Méditerranée, 13009 Marseille, France

^dHoward Hughes Medical Institute, Massachusetts Institute of Technology, Cambridge, MA 02139, United States

^eCanadian Institute for Advanced Research, Bio-inspired Solar Energy Program, Toronto, ON M5G 1M1, Canada

Abstract

Carbon monoxide dehydrogenase (CODH) plays an important role in the processing of the one-carbon gases carbon monoxide and carbon dioxide. In CODH enzymes, these gases are channeled to and from the Ni-Fe-S active sites using hydrophobic cavities. In this work, we investigate these gas channels in a monofunctional CODH from *Desulfovibrio vulgaris*, which is unusual among CODHs for its oxygen-tolerance. By pressurizing *D. vulgaris* CODH protein crystals with xenon and solving the structure to 2.10 Å resolution, we identify 12 xenon sites per CODH monomer, thereby elucidating hydrophobic gas channels. We find that *D. vulgaris* CODH has one gas channel that has not been experimentally validated previously in a CODH, and a second channel that is shared with *Moorella thermoacetica* carbon monoxide dehydrogenase/acetyl-CoA synthase (CODH/ACS). This experimental visualization of *D. vulgaris* CODH gas channels lays groundwork for further exploration of factors contributing to oxygen-tolerance in this CODH, as well as study of channels in other CODHs. We dedicate this publication to the memory of Dick Holm, whose early studies of the Ni-Fe-S clusters of CODH inspired us all.

This is an open access article under the CC BY-NC-ND license (<http://creativecommons.org/licenses/by-nc-nd/4.0/>).

*Corresponding author at: Massachusetts Institute of Technology, Dept. of Biology, Cambridge, MA 02139, United States. cdrennan@mit.edu (C.L. Drennan).

Author contributions

*Dv*CODH protein was prepared by SD; all crystallographic experiments were carried out by AB; structure analysis was performed by AB and CLD. AB wrote the manuscript with edits from CLD.

Declaration of Competing Interest

The authors declare no competing financial interests.

Appendix A. Supplementary data

Supplementary data to this article can be found online at <https://doi.org/10.1016/j.jinorgbio.2022.111774>.

Keywords

CO-dehydrogenase; Carbon monoxide; Crystallography; Xenon; Gas channels; Tunnels

1. Introduction

Ni-Fe-S-dependent carbon monoxide dehydrogenases (CODHs) catalyze the reversible oxidation of CO to CO₂ at a Ni-Fe-S center called the C-cluster in the biological equivalent of the water-gas shift reaction ($\text{CO} + \text{H}_2\text{O} \rightleftharpoons \text{CO}_2 + 2\text{H}^+ + 2\text{e}^-$). In addition to their intriguing chemical properties, Ni-Fe-S-dependent CODHs have potential for removing pollutants from the environment. Globally, CODHs eliminate approximately 10⁸ tons of CO from the environment each year and contribute to the production of 10¹¹ tons of acetate per year from CO₂ [1–3]. Each CODH homodimer contains five metallocofactors: two B-clusters, two C-clusters, and one D-cluster [4,5]. The C-cluster is the site of reversible CO₂ reduction to CO, whereas the B- and D-clusters of CODH are responsible for wiring electrons to the C-cluster for CO₂ reduction. CODHs are employed by microbes in a variety of metabolic roles, including in methanogenesis and acetogenesis. Depending on the metabolic role, CODHs can be found as standalone proteins or as part of larger enzyme complexes; to reflect these variations, CODHs can be divided into four classes. Classes I and II are found in methanogens, with class I enzymes being involved in autotrophic methanogenesis whereas class II enzymes are involved in acetoclastic methanogenesis [6]. Methanogenic CODHs form a stable 40-meric complex that includes acetyl-CoA synthase (ACS) and corrinoid-iron sulfur protein (CFeSP), called the acetyl-CoA decarbonylase/synthase complex (ACDS). Although ACDS is known to form an ($\alpha_2\epsilon_2$)₄ β_8 ($\gamma\delta$)₈ complex of four $\alpha_2\epsilon_2$ CODH tetramers, eight β ACS monomers, and eight $\gamma\delta$ CFeSP dimers, the overall architecture and organization of these subunits remains unknown [7,8]. Class III CODHs are found in acetogens and form a heterotetrameric complex with ACS (CODH/ACS) [6]. In acetogenic bacteria, CODH/ACS generates acetyl-CoA from CO₂ through the Wood-Ljungdahl pathway. ACS utilizes an additional Ni-Fe-S metallocofactor termed the A-cluster to join the CO molecule that is produced at the C-cluster of CODH with a methyl group that is provided through a transient interaction with CFeSP [9–13]. Class IV CODHs, such as the *Desulfovibrio vulgaris* CODH (*Dv*CODH) used in this study, form a monofunctional homodimer, which catalyzes the reversible oxidation of CO to CO₂ [6].

The CODH from *D. vulgaris* has an interesting and unique property of oxygen-tolerance. *Dv*CODH is the most oxygen-tolerant of any known CODH [14–16]. Although the *Carboxydotherrmus hydrogenoformans* CODH II (*Ch*CODH II) appears to have some tolerance to oxygen, *Dv*CODH reacts with O₂ half as fast as *Ch*CODH II, and recovers much more activity after O₂ removal. Importantly, *Dv*CODH can be fully reactivated upon reduction, whereas reduction of *Ch*CODH II after O₂ gives only 20% activity [14]. The survival time of *Dv*CODH after oxygen exposure is quite long, as *Dv*CODH retains all metallocofactors after 2 days of oxygen exposure [15]. Following exposure to oxygen, the C-cluster of *Dv*CODH undergoes a rearrangement giving a novel oxidized C-cluster conformation. With an oxidized C-cluster, *Dv*CODH is inactive, but this C-cluster rearrangement is fully reversible such that upon reduction the C-cluster returns to its

canonical reduced conformation [16]. Due to its interesting and unique properties, we have pursued the further characterization of the CODH from *D. vulgaris* to determine how various features of this enzyme resemble or differ from other CODHs. Here, we examine internal cavities that are proposed to be used for gas transport within *Dv*CODH.

The first channel in an enzyme structure was reported in 1988 for tryptophan synthase [17]. Since then, internal cavities have been discovered in a large number of enzyme structures [18]. Cavities can provide access for substrates and products between the protein surface and a buried active site, and, in some cases, modulate enzyme specificity [18]. For the latter, channels have become an area of interest for protein engineering [19]. In the case of enzymes with two active sites, a channel can protect a reactive intermediate as it travels between active sites, decrease transit time, and prevent intermediate loss [20,21]. CODHs are known to use channels to route gaseous molecules to and from their active sites [22–25]. The cavity search program CAVER [26] predicts that the route of these gas channels will vary in different CODHs for which structures have been determined (Fig. 1). There appears to be a common path for gas channels in monofunctional CODHs, whereas in bifunctional CODH/ACS, the path of the channels varies significantly based on the quaternary structure of the enzyme. Whereas the gas channel of *Clostridium autoethanogenum* CODH/ACS (*Ca*CODH/ACS) is predicted to be similar to those found in monofunctional CODHs, the path of the gas channel is entirely distinct in CODH/ACS from *Moorella thermoacetica* (*Mt*CODH/ACS). Although it is likely that gas channels will connect the metallocluster active sites in methanogenic ACDS complexes, the arrangements of CODH subunits to ACS subunits is currently unknown.

Cavity calculations have been completed on various CODHs, however, experimental data showing the path of gas channels in CODHs are limited. In this study, we perform crystallographic studies with xenon gas to experimentally visualize the gas channel of *Dv*CODH. Xenon is a useful crystallographic tool in that it is known to bind in hydrophobic cavities, ligand and substrate binding sites, and channel pores. Therefore xenon can be used to identify these features [31,32]. For this system, xenon is considered a reasonable mimic for CO due to their similar sizes. Xenon has a van der Waals radius of 2.16 Å, similar to the effective van der Waals radius of CO, which is ~2 Å. Another useful parameter for comparing the sizes of these gases is kinetic diameter, which is typically used to evaluate the likelihood of collision, adsorption, and permeation of gases into porous materials [33]. The kinetic diameters for xenon and CO are 4.05 Å and 3.76 Å respectively [33,34]. Interestingly, the kinetic diameter of CO₂ is only 3.30 Å, which suggests that cavities permeable to xenon and CO would also be permeable to CO₂ [33]. Xenon's comparable size to CO and CO₂ along with its ability to bind in hydrophobic cavities make xenon gas a suitable tool for studying the gas channels of CODHs. Previously in two different studies, xenon was used to identify the hydrophobic gas channels in *Mt*CODH/ACS, elucidating a 138 Å long channel used for CO transport [22,35]. Xenon was also used to map gas channels in a methanogenic $\alpha_2\epsilon_2$ CODH complex [30], although the structure with xenon was not deposited in the PDB. Here, we present the xenon-bound structure of the monofunctional *Dv*CODH and compare it to the one deposited xenon-bound *Mt*CODH/ACS structure [22].

2. Materials and methods

2.1. Protein purification

*Dv*CODH was expressed in the presence of the C-cluster maturation factor *CooC*, as described previously [15,16,36,37]. Briefly, the *cooS* gene encoding CODH and the *cooC* gene encoding the *CooC* maturase were cloned into modified pBGF4 shuttle vectors under the control of the promoter of the *Desulfovibrio fructosovorans* Ni-Fe hydrogenase operon. The CODH construct was N-terminally strep-tagged. The protein expressed was in *D. fructosovorans* str. MR400 [38] and purified under anaerobic conditions in a Jacomex anaerobic chamber (100% N₂ atmosphere) by affinity chromatography on Strep-Tactin Superflow resin, as described previously [36]. Protein concentrations were determined by amino acid analysis at the Centre for Integrated Structural Biology (Grenoble, France).

2.2. Growth and pressurization of *Dv*CODH crystals with Xenon

Crystals were grown anaerobically (100% N₂ atmosphere) at 21 °C by hanging drop vapor diffusion in an MBraun anaerobic chamber. The hanging drop consisted of 0.75 μL of protein solution (CODH at 10 mg/mL in 100 mM Tris-HCl pH 8) mixed with 1 μL of reservoir solution (250 mM MgCl₂, 16% (w/v) PEG 3350), with the addition of 0.25 μL of a solution of crushed microcrystals to aid in nucleation (at a 1:100,000 dilution from a seed stock). Diffraction quality crystals grew within 7 days. Crystals belong to space group *C2* with a monomer in the asymmetric unit ($a = 113.8 \text{ \AA}$, $b = 100.9 \text{ \AA}$, $c = 65.4 \text{ \AA}$, $\beta = 124.9^\circ$). Crystals were cryoprotected with 250 mM MgCl₂, 20% (w/v) PEG 3350, 9% (v/v) glycerol. A Xe pressure cell built based on the design from the Stanford Synchrotron Radiation Lightsource (SSRL) [39] was used to pressurize the crystals with Xe following cryoprotection but before cryocooling, according to standard protocols [39]. Briefly, a looped and cryoprotected crystal was lowered into the pressurizing chamber, and the chamber was closed (Fig. S1). To prevent the crystal from drying out, a vial containing ~100 μL of water was placed at the bottom of the pressurizing chamber. The chamber was pressurized with 200–300 psi Xe gas for 16 min. After quickly depressurizing the chamber (~20 s), the looped crystal was plunged into liquid nitrogen.

2.3. Data collection and processing

Native data (wavelength = 0.9791 Å) were collected at the Advanced Photon Source (Argonne, IL) at beamline 24-ID-C using an Eiger-2 16 M detector. Xe peak data (wavelength = 2.0663 Å) were collected at the SSRL beamline 9–2 using a Dectris Pilatus 6 M detector. All data were integrated and scaled in XDS [40]. Data collection statistics are summarized in Table 1.

2.4. Structure determination and refinement

The initial structure of xenon-pressurized *Dv*CODH was determined to 2.10 Å resolution by molecular replacement (MR) in the program Phaser [41]. The search model for MR was generated from the structure of the CODH from *Desulfovibrio vulgaris* (100% sequence identity; PDB ID: 6B6V, *P2*₁*2*₁*2*₁, $a = 65.65 \text{ \AA}$, $b = 111.96 \text{ \AA}$, $c = 195.29 \text{ \AA}$) by modification in Sculptor [42] using the Schwarzenbacher algorithm [43] with a pruning level of 2.

Residues 4–628 (of 629 total) were used in the search model, including only one monomer. A single MR solution was found with an LLG of 3270, TFZ of 55.9, and *R*-value of 34.9. For this structure, refinement of atomic coordinates and atomic displacement parameters (*B*-factors) was carried out in Phenix. Custom parameter files were used to restrain C-cluster geometry during refinement. The model was completed through iterative rounds of model building in Coot [44] and refinement in Phenix [45]. In advanced stages of refinement, water molecules were added in Coot and verified using a composite omit map. Final stages of refinement included translation, libration, screw (TLS) parameterization with one TLS group per monomer [46]. Model was refined without hydrogens.

Following initial rounds of refinement, unaccounted for electron density in the $2|F_o| - |F_c|$ maps calculated from the native diffraction data was present in the hydrophobic cavities. Anomalous difference maps calculated from diffraction data collected at the xenon peak wavelength (2.0663 Å) showed consistent high σ electron density peaks. Into these electron density peaks, Xe atoms were modeled in Coot.

Final refinement of each structure yielded models with low free *R*-factors, reasonable stereochemistry, and small root mean square deviations from ideal values for bond lengths and angles. The final model contains residues 8–628 (of 629 total). Model was validated using simulated annealing composite omit maps calculated in Phenix. Model geometry was analyzed using MolProbity [47]. Analysis of Ramachandran statistics indicated that each structure contained the following percentages of residues in the favored, allowed, and disallowed regions, respectively: 96.3%, 3.4%, 0.3%. Figures were generated in PyMOL [48]. Crystallography packages were compiled by SBGrid [49].

2.5. Computational channel prediction

Internal channel prediction was performed by CAVER [26] by applying a probe radius of 0.9 Å.

3. Results

3.1. The gas channels of DvCODH

Using our in-house xenon pressure cell, we have determined the structure of xenon-bound DvCODH to 2.10 Å resolution (Fig. 2). Alignment of the xenon-gassed DvCODH with the non-gassed structure (6B6W) [16] reveals a high level of similarity, with a C α r.m.s.d. of 0.351 Å and no substantial side chain movements (Fig. S2). The structure of xenon-bound DvCODH reveals 12 xenon sites per monomer as found in the asymmetric unit, equating to 24 xenon sites per CODH dimer, which is the biologically relevant oligomeric state. These 12 xenon atoms appear to form a forked channel, leading in one direction toward the dimer interface (sites 1–4) and in the other direction away from the dimer interface (sites 5–12). Both routes (sites 1–4 and sites 5–12) are directed toward the C-cluster, suggesting that CO may access the active site through either of these channels. In a deviation from the CAVER [26] predictions, the gas channels of the two CODH monomers are not joined. This observation is consistent with the findings in MvCODH/ACS, wherein an internal channel was predicted to connect the two C-clusters but there were no xenon sites identified between

the C-clusters. In *Dv*CODH, it appears that xenon atoms are excluded from this region due to the presence of water molecules found within this predicted channel and polar residues lining this predicted channel (Fig. S3). These water molecules and polar residues would likely also repel CO/CO₂. Additionally, xenons 10–12 are outside of the CAVER channel prediction, but aside from these deviations, the experimental data show strong agreement with the CAVER calculations, as 9 xenon sites are within the predicted channel.

3.2. Xenon binding cavities are predominantly hydrophobic

As expected, the vast majority of amino acid residues surrounding the xenon sites in *Dv*CODH are hydrophobic (Fig. 3). There are 58 amino acids in total within 5 Å of the 12 xenon sites. Of these 58 amino acids, 46 are nonpolar aliphatic (79%), 5 are aromatic (9%), 6 are polar (10%), and 1 is charged (2%). The single charged residue, H572, is oriented such that its side chain points away from the channel, and in fact the only portion of H572 that comes within 5 Å of the nearby xenon site 5 is the backbone. One of the aromatic residues, Y563 (contacting site 6), also contains a polar hydroxyl group, which does point inward toward the channel. The six polar contacting residues include: T210 (site 1), N522 (site 6), C529 (sites 7 and 8), S548 (site 5), S549 (site 5), and T571 (site 5). For both threonine residues, T210 and T571, the hydroxyl group is pointing away from the channel and the methyl group points in toward the channel. S548 similarly has its hydroxyl group facing outward such that it does not contact the xenon cavities; S549 on the other hand has its polar hydroxyl group oriented toward the channel. The final two sites, N522 and C529, also have polar groups pointing into the channel. However, these residues only make up a small subset of those coming into contact with the channel, with the majority of channel-forming residues being hydrophobic amino acids, such as leucine, isoleucine, valine, and phenylalanine.

3.3. Similarities and differences of gas channels in *D. vulgaris* and *M. thermoacetica*

As predicted by CAVER, there are notable variations between the gas channels of *Dv*CODH and *Mt*CODH/ACS; however, there are also similarities (Fig. 4). Variations can be rationalized by the fact that channels in *Mt*CODH/ACS have an additional purpose: to transport gas between active sites. *Dv*CODH, a monofunctional enzyme, serves to catalyze the reversible oxidation of CO to CO₂ at the C-cluster, whereas the bifunctional *Mt*CODH/ACS utilizes two active sites, the C-cluster and the A-cluster, to catalyze the reversible reduction of CO₂ to CO and the synthesis of acetyl-CoA from CO, CH₃, and CoA. Therefore, in *M. thermoacetica*, the channels must direct the CO product from one active site, the C-cluster, to another active site, the A-cluster. In contrast, in *D. vulgaris*, the channels simply direct entry to and exit from the active site. The differences in the functions of these channels are reflected in the experimentally observed path of these channels.

In *Mt*CODH/ACS all channels observed are internal, connecting the C- and A-clusters. In other words, there were no xenon sites identified in *Mt*CODH/ACS that would allow for gaseous substrates to exit the C-cluster and reach the protein surface. The lack of exit channels in this particular conformation of CODH/ACS is a valuable feature because it assists in ensuring that all of the CO generated at the C-cluster is directed to the A-cluster. CODH/ACS is known to be a dynamic enzyme complex, so it is probable that conformational changes in the CODH/ACS heterotetramer would expose a path for CO₂

entry to the C-cluster, which may not be accessible in this conformation. The gas channel of *Dv*CODH has two branches, both of which lead to the surface of the enzyme and could serve for entry and exit of gaseous substrates and products. It is probable that one branch is used for CO entry and the other branch is used for CO₂ exit, though there is no clear indication from the experimental data which branch is used for entry and which is used for exit.

Of the two branches of the gas channel from *Dv*CODH, one branch is shared with *Mi*CODH/ACS whereas the other branch veers in a distinct direction (Fig. 4). The similarity in location of xenon sites 1–5 of *Dv*CODH and the CODH xenon sites of *Mi*CODH/ACS would suggest some sequence conservation of channel residues. Recall that in *Dv*CODH, 58 residues contact xenon sites. In *Mi*CODH 42 residues contact xenon sites (there are additional contacts in ACS as well). *Dv*CODH and *Mi*CODH share 25 xenon contacts in common. Of these 25 common contacts, 11 (44%) are conserved, having the same amino acid in both enzymes at the same position. Although there is substantial variation in the identity of the channel residues, biochemical properties of these channel residues show moderate conservation, with 17 of 25 (68%) common contacts share similar biochemical properties (both nonpolar aliphatic, both aromatic, or both polar) in *Dv*CODH and *Mi*CODH.

In addition to showing common contacts, overlaying the two xenon-bound CODH structures provides insight into where these channels differ and why we see a different path for the gas channel in *Dv*CODH that is not found in *Mi*CODH/ACS. Particularly, we note that upon aligning these structures we see that several residues from *Mi*CODH/ACS occupy the same positions as the xenon sites from *Dv*CODH. Particularly the following residues from *Mi*CODH clash with xenon sites from *Dv*CODH: L620 (site 2), F634 (site 3), W595 (site 6), F576 (site 7), M563 (site 8), and N453 (site 9) (Fig. 4E). Notably, despite the clashes of L620 and F634 of *Mi*CODH with xenon sites in *Dv*CODH, there are still xenon sites nearby these residues in *Mi*CODH (sites 1–5 in Fig. 4C) forming a channel analogous to that found in *Dv*CODH (sites 1–5 in Fig. 4B). In contrast, the clashes of *Mi*CODH residues W595, F576, M563, and N453 with xenon sites of *Dv*CODH do give rise to channel blockage. There are no *Mi*CODH xenon sites near xenon sites 6–12 in *Dv*CODH, indicating that no such channel exists in this region of *Mi*CODH. This difference appears to be due to bulky residues protruding out and blocking the space where this channel forms in *Dv*CODH. Overall, it appears that *Dv*CODH shares the channel present in *Mi*CODH that is directed toward the A-cluster (Fig. 4A), and *Dv*CODH has an additional channel, potentially with one channel serving as the path for substrate entry and the other as the path for product exit.

4. Discussion

Through this work, we have elucidated the path of gas channels in *Dv*CODH (Fig. 2). These gas channels in the monofunctional *Dv*CODH appear to have some similarity to the channels of bifunctional *Mi*CODH/ACS, sharing one channel in common, but *Dv*CODH has an additional channel not found in *Mi*CODH/ACS (Fig. 4). To date, *Dv*CODH and *Mi*CODH/ACS are the only two CODHs for which xenon-bound structures have been deposited in the PDB. Hydrophobic gas channels have been characterized with xenon-

soaking studies in other CODHs, such as the methanogenic CODH, but their structures were not deposited in the PDB, making detailed structural comparisons challenging [30,35]. We remain interested in how gas channels vary in CODHs more broadly. Thus, to gain insight into potential similarities and differences of gas channels in other CODHs, we can use sequence and structural comparisons.

Here, we align the sequence of *Dv*CODH with those of other monofunctional CODHs for which a structure has been deposited in the PDB (*R. rubrum*: 1JQK, *C. hydrogenoformans* type II: 1SU6, *C. hydrogenoformans* type IV, 6ELQ), and we align the *Dv*CODH sequence with those of bifunctional CODHs that have been visualized in complex with their corresponding ACS subunit (*M. thermoacetica*: 1MJG, and *C. autoethanogenum*: 6YTT). For all of these CODHs, we note sequence similarities and differences at the positions of the 58 channel-forming amino acids in *Dv*CODH (Figs. 5–6, S4–S5). The cavity search program CAVER predicts that the channels of *Dv*CODH are analogous to those of other monofunctional CODHs from *R. rubrum*, *C. hydrogenoformans* type II, and *C. hydrogenoformans* type IV (Fig. 1). Upon aligning the sequences of these four monofunctional CODHs, we see that each *R. rubrum*, *C. hydrogenoformans* type II, and *C. hydrogenoformans* type IV CODH have the same amino acid or an amino acid similar in biochemical properties at the equivalent position for minimally 48 of the 58 residues (83%) contacting xenon in *Dv*CODH (Figs. 5–6). Despite their high sequence similarity, there are some differences between *Dv*CODH and other monofunctional CODHs. In *Dv*CODH, we observe an alanine at position 589, contacting xenon site 2 (Fig. 3A). However, at the equivalent position in *R. rubrum* CODH (residue 601), we observe a valine. The larger size of this valine sidechain is significant because V601 of *R. rubrum* CODH clashes with xenon site 2 upon overlaying the two structures (Figs. 5, 6A). Interestingly, we see a similar pattern in all other CODHs analyzed here, wherein at the position equivalent to A589 in *Dv*CODH, there is a larger nonpolar residue. Specifically, at this position there is a leucine in *C. hydrogenoformans* type II, *C. hydrogenoformans* type IV, *M. thermoacetica*, and *C. autoethanogenum* CODHs (Figs. 5, 6B–E). Although the valine and leucine residues in this position all clash with xenon site 2, it is not clear that this clash is sufficient to block the channel. As noted previously, in *Mt*CODH the clash of L620 (the equivalent position of *Dv*CODH A589) with xenon site 2 does not preclude the formation of a gas channel with a similar path (Fig. 4). Aside from a slight shift in the positions of the xenon atoms, the channel represented by xenon sites 1–5 in *Mt*CODH appears comparable to the one represented by xenon sites 1–5 in *Dv*CODH. Therefore, it is reasonable to expect that the clashes found between xenon site 2 and residues at the equivalent position to *Dv*CODH A589 do not block any gas channels. Since there are no additional clashes found in *R. rubrum*, *C. hydrogenoformans* type II, or *C. hydrogenoformans* type IV, it is probable that all channels present in *Dv*CODH exist in these other monofunctional CODHs.

In bifunctional CODH/ACS, upon alignment with xenon-bound *Dv*CODH we observe additional clashes with the xenon sites of *Dv*CODH. As described previously, W595, F576, M563, and N453 of *Mt*CODH (aligning with contacting residues A564, V545, L532, and I431 of *Dv*CODH, respectively) do appear to block the gas channel represented by xenon sites 6–12 in *Dv*CODH (Figs. 4, 5, 6D), which is consistent with CAVER predictions (Fig. 1). For the CODH/ACS from *C. autoethanogenum*, alignment with xenon-bound *Dv*CODH

suggests that the channel represented by xenon sites 1–5 in *Dv*CODH is less accessible even though CAVER maps out this region as a cavity in both of these enzymes. Although we expect L593 of *Ca*CODH/ACS (which aligns with *Dv*CODH A589) is insufficient to block this putative gas channel in spite of its clash with xenon site 2, there is an additional clash of W600 (aligned with *Dv*CODH V596) with xenon site 1 of *Dv*CODH (Figs. 5, 6E). Therefore, W600 of *Ca*CODH/ACS may help to direct CO toward the other cavity that leads to the ACS subunit, preventing loss of CO from the enzyme before it can be utilized in the production of acetyl-CoA. In contrast to the channel represented by xenon sites 1–5, there are no clashes between *Ca*CODH/ACS and xenon sites 6–12 of *Dv*CODH, which comprise the channel that would lead to ACS in *C. autoethanogenum* (Fig. 6E). Thus, if the putative gas channel represented by xenon sites 1–5 is used in *Ca*CODH/ACS, it is not likely to be employed as a pathway for CO. Previously, it was suggested that CO₂ may access the C-cluster of CODH through this path [24]. The channel represented by xenon sites 6–12, on the other hand, is likely to be the primary channel in *Ca*CODH/ACS that is responsible for directing the CO from the C-cluster to the A-cluster in the ACS subunit.

To investigate the conservation of channel blocking residues in bifunctional CODH/ACSs, we completed a sequence and BLAST distance tree analysis of thirteen additional putative CODHs (that have not been structurally characterized) from bacteria that are proposed acetogens and/or have a corresponding putative ACS in their genome (Fig. S6) [56,57]. From this analysis, we found that for the proposed channel-blocking residues in *M. thermoacetica* (W595, F576, M563, and N453), W595 is conserved in all *Moorella* species analyzed, and F576, M563, and N453 are conserved within the *Moorella* genus as well as in *Thermoanaeromonas toyohensis* and *Thermoanaerobacteraceae* bacteria, which show the closest relation to the *Moorella* genus in our BLAST distance tree analysis. For W600, the proposed channel-blocking residue in *C. autoethanogenum*, we note conservation within all *Clostridium* species analyzed, as well as conservation of aromatic character within the *Clostridiales* order (*Clostridium* and *Acetobacterium* genus), indicating that channel blocking may be conserved among this order.

In addition to channels providing routes for substrates into and out of buried active sites and/or between active sites, channels can also influence substrate selectivity. When the active site is an oxygen-sensitive metallocofactor and the substrate is a gaseous molecule, the question that follows is whether channels can select for the gaseous substrate and limit entry of molecular oxygen gas that will damage the metallocofactor. Although the role of channels in CODHs in regard to oxygen permeability is only beginning to be investigated, research on [NiFe] and [FeFe] hydrogenases is further advanced [50–53]. For example, studies have shown that substituting methionines in a highly conserved gas channel for a leucine and a valine generates an oxygen-tolerant [NiFe] hydrogenase [54]. Given that *Dv*CODH is known to be more tolerant to molecular oxygen than other CODH enzymes (see Introduction), we were interested to determine if *Dv*CODH had evolved distinct gas channels from those channels observed in other CODHs. As reported above, we do not find substantial differences in the gas channels. Thus, the largest difference between *Dv*CODH and the other CODHs described in this study is still the presence of a more oxygen-stable [2Fe–2S] D-cluster in the *Dv* enzyme [15,16]. Despite the lack of a novel gas channel in *Dv*CODH, smaller differences revealed in the residues lining these

channels may still be important for *Dv*CODH oxygen stability. As the above example from the hydrogenase literature illustrates, small changes in amino acids can have a meaningful impact. Computational methodology has advanced to allow for extensive mapping of diffusion channels in hydrogenases [55]. A similar approach could be employed using the data provided here, potentially allowing for more conservative residue substitutions to be identified as potentially contributing to the observed oxygen stability of *Dv*CODH.

5. Conclusions

From the xenon gas studies on CODHs performed thus far, there appear to be two main gas routes: one spanning from the C-cluster toward the interface of the CODH homodimer (as observed in *Dv*CODH xenons 1–5 and *Mi*CODH/ACS) and another leading from the C-cluster away from the CODH dimer interface (as observed in *Dv*CODH xenons 6–12 and not in *Mi*CODH/ACS). *C. autoethanogenum* CODH/ACS, on the other hand, is likely to use the latter channel (xenons 6–12), consistent with the alternative positioning of its ACS subunit. Specific amino acid residues can block the path of the gas channels, allowing the enzyme to control the flow of CO in one specific direction, such as in the direction of the A-cluster in the case of bifunctional CODH/ACSs. Often aromatic residues such as tryptophan and phenylalanine are used as channel-blocking residues. In the other monofunctional CODHs for which structures are available, our analysis suggests that both gas channels are available for CO (or possibly CO₂) gas to enter/exit the enzymes. We know the least about gas channels in methanogenic ACDS complexes that are comprised of ($\alpha_2\epsilon_2$)₄ β_8 ($\gamma\delta$)₈ subunits [7,8]. Chan and co-workers have provided a crystal structure of two of the subunits, $\alpha_2\epsilon_2$, in complex [30], but there is no structure of the CODH (α) subunit with an ACS (β) subunit available, limiting our ability to predict likely routes for CO gas to travel. It is also unknown how channel variations affect oxygen sensitivity. Further experimental study will be crucial to advancing our understanding of gas channeling in CODHs.

Supplementary Material

Refer to Web version on PubMed Central for supplementary material.

Acknowledgements

The authors thank Elizabeth C. Wittenborn (MIT) for advice on crystallization conditions, Rebekah E. Bjork (MIT) for assistance with xenon pressurization, and Lindsey R. F. Backman (MIT) for assistance with data processing. We additionally thank Douglas C. Rees and the Stanford Synchrotron Radiation Laboratory (SSRL) for conceptualization of the xenon pressure cell design, which was replicated in the Drennan Laboratory with assistance from the MIT Central Machine Shop and Rebekah Bjork. This work was supported by National Institutes of Health Grants R35 GM126982 (to CLD) and funded by the Centre National de la Recherche Scientifique, Aix Marseille University and the French Agence Nationale de la Recherche (ANR-15-CE05-0020 and ANR-17-CE11-0027). CLD is a Howard Hughes Medical Institute Investigator and a fellow of the Bio-inspired Solar Energy Program, Canadian Institute for Advanced Research. SD is a part of FrenchBIC. This work is based on research conducted at the Advanced Photon Source on the Northeastern Collaborative Access Team beamlines, which are funded by the National Institute of General Medical Sciences from the NIH (P41 GM103403). The Eiger2 16M detector on beamline 24-ID-C is funded by a NIH Office of Research Infrastructure Programs High End Instrumentation grant (S10 RR029205). This research used resources of the Advanced Photon Source, a U.S. Department of Energy (DOE) Office of Science User Facility operated for the DOE Office of Science by Argonne National Laboratory under Contract No. DE-AC02-06CH11357. This work is also based on research conducted at the Stanford Synchrotron Radiation Laboratory (SSRL). SSRL, a national user facility, is operated by Stanford University on behalf of the U.S. Department of Energy, Office of Basic Energy Sciences. The SSRL Structural Molecular Biology Program is supported by the Department of Energy, Office of Biological

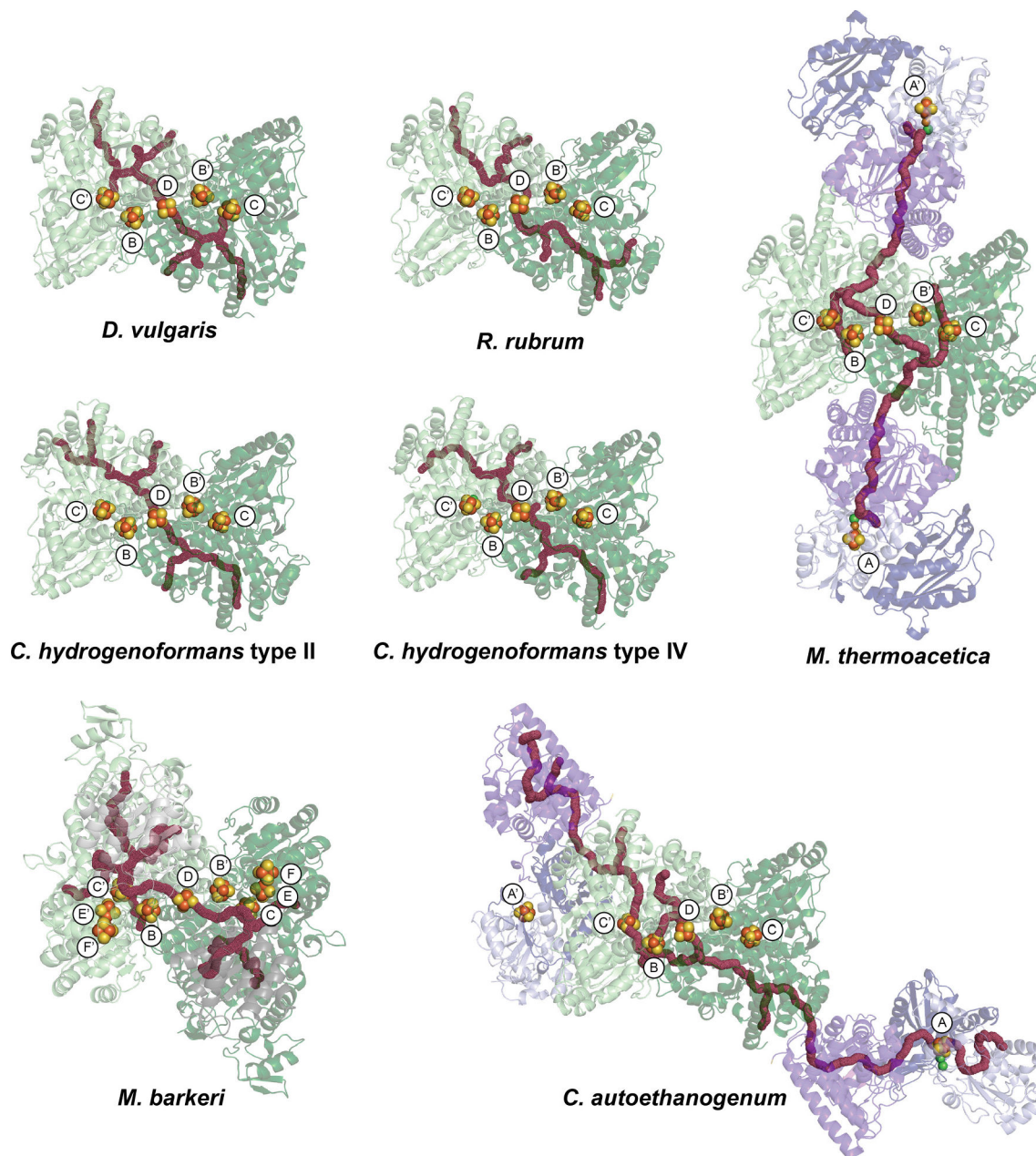
and Environmental Research, and by the National Institutes of Health, National Center for Research Resources, Biomedical Technology Program, and the National Institute of General Medical Sciences.

References

- [1]. Bartholomew G, Alexander M, Microbial metabolism of carbon monoxide in culture and in soil, *Appl. Environ. Microbiol* 37 (5) (1979) 932–937. [PubMed: 485139]
- [2]. Drake HL, Acetogenesis, acetogenic bacteria, and the acetyl-CoA “Wood/Ljungdahl” pathway: past and current perspectives, in: *Acetogenesis*, Springer, 1994, pp. 3–60.
- [3]. Zamble D, Rowi ska- yrek M, Kozlowski H, *The Biological Chemistry of Nickel*, 2017, pp. 1–380.
- [4]. Dobbek H, Svetlitchnyi V, Gremer L, Huber R, Meyer O, Crystal structure of a carbon monoxide dehydrogenase reveals a [Ni-4Fe-5S] cluster, *Science* 293 (2001) 1281–1285. [PubMed: 11509720]
- [5]. Drennan CL, Heo J, Sintchak MD, Schreiter E, Ludden PW, Life on carbon monoxide: X-ray structure of *Rhodospirillum rubrum* Ni-Fe-S carbon monoxide dehydrogenase, *Proc. Natl. Acad. Sci. U. S. A* 98 (2001) 11973–11978. [PubMed: 11593006]
- [6]. Lindahl PA, The Ni-containing carbon monoxide dehydrogenase family: light at the end of the tunnel? *Biochemistry* 41 (2002) 2097–2105. [PubMed: 11841199]
- [7]. Grahame DA, Catalysis of acetyl-CoA cleavage and tetrahydrosarcinapterin methylation by a carbon monoxide dehydrogenase-corrinoid enzyme complex, *J. Biol. Chem* 266 (1991) 22227–22233. [PubMed: 1939246]
- [8]. Kocsis E, Kessel M, DeMoll E, Grahame DA, Structure of the Ni-Fe-S protein subcomponent of the acetyl-CoA decarbonylase/synthase complex from *Methanosarcina thermophila* at 26-Å resolution, *J. Struct. Biol* 128 (1999) 165–174. [PubMed: 10600570]
- [9]. Drake HL, Gössner AS, Daniel SL, Old Acetogens, new light, *Ann. N. Y. Acad. Sci* 1125 (2008) 100–128. [PubMed: 18378590]
- [10]. Ljungdahl LG, A life with Acetogens, thermophiles, and cellulolytic anaerobes, *Annu. Rev. Microbiol* 63 (2009) 1–25. [PubMed: 19575555]
- [11]. Menon S, Ragsdale SW, Evidence that carbon monoxide is an obligatory intermediate in anaerobic acetyl-CoA synthesis, *Biochemistry* 35 (1996) 12119–12125. [PubMed: 8810918]
- [12]. Ragsdale SW, Pierce E, Acetogenesis and the Wood-Ljungdahl pathway of CO₂ fixation, *Biochim. Biophys. Acta* 1784 (2008) 1873–1898. [PubMed: 18801467]
- [13]. Ragsdale SW, Wood HG, Antholine WE, Evidence that an iron-nickel-carbon complex is formed by reaction of CO with the CO dehydrogenase from *Clostridium thermoaceticum*, *Proc. Natl. Acad. Sci. U. S. A* 82 (1985) 6811–6814. [PubMed: 2995986]
- [14]. Merrouch M, Hadj-Saïd J, Domnik L, Dobbek H, Léger C, Dementin S, Fourmond V, O₂ inhibition of Ni-containing CO dehydrogenase is partly reversible, *Chem. Eur. J* 21 (52) (2015) 18934–18938. [PubMed: 26568460]
- [15]. Wittenborn EC, Guendon C, Merrouch M, Benvenuti M, Fourmond V, Léger C, Drennan CL, Dementin S, The solvent-exposed Fe–S D-cluster contributes to oxygen-resistance in *Desulfovibrio vulgaris* Ni–Fe carbon monoxide dehydrogenase, *ACS Catal* 10 (2020) 7328–7335. [PubMed: 32655979]
- [16]. Wittenborn EC, Merrouch M, Ueda C, Fradale L, Léger C, Fourmond V, Pandelia M-E, Dementin S, Drennan CL, Redox-dependent rearrangements of the NiFeS cluster of carbon monoxide dehydrogenase, *eLife* 7 (2018), e39451. [PubMed: 30277213]
- [17]. Hyde CC, Ahmed SA, Padlan EA, Miles EW, Davies DR, Three-dimensional structure of the tryptophan synthase $\alpha_2\beta_2$ multienzyme complex from *salmonella typhimurium*, *J. Biol. Chem* 263 (33) (1988) 17857–17871. [PubMed: 3053720]
- [18]. Pravda L, Berka K, Svobodová Va eková R, Sehnal D, Banáš P, Laskowski RA, Ko a J, Otyepka M, Anatomy of enzyme channels, *BMC Bioinformatics* 15 (1) (2014) 379. [PubMed: 25403510]
- [19]. Kokkonen P, Bednar D, Pinto G, Prokop Z, Damborsky J, Engineering enzyme access tunnels, *Biotechnol. Adv* 37 (6) (2019), 107386. [PubMed: 31026496]

- [20]. Miles EW, Rhee S, Davies DR, The molecular basis of substrate channeling, *J. Biol. Chem* 274 (18) (1999) 12193–12196. [PubMed: 10212181]
- [21]. Bera AK, Smith JL, Zalkin H, Dual role for the glutamine Phosphoribosylpyrophosphate Amidotransferase Ammonia Channel: Interdomain signaling and intermediate channeling, *J. Biol. Chem* 275 (11) (2000) 7975–7979. [PubMed: 10713115]
- [22]. Doukov TI, Blasiak LC, Seravalli J, Ragsdale SW, Drennan CL, Xenon in and at the end of the tunnel of bifunctional carbon monoxide dehydrogenase/acetyl-CoA synthase, *Biochemistry* 47 (2008) 3474–3483. [PubMed: 18293927]
- [23]. Maynard EL, Lindahl PA, Evidence of a molecular tunnel connecting the active sites for CO₂ reduction and acetyl-CoA synthesis in acetyl-CoA synthase from *Clostridium thermoaceticum*, *J. Am. Chem. Soc* 121 (39) (1999) 9221–9222.
- [24]. Lemaire ON, Wagner T, Gas channel rerouting in a primordial enzyme: structural insights of the carbon-monoxide dehydrogenase/acetyl-CoA synthase complex from the acetogen *Clostridium autoethanogenum*, *Biochim. Biophys. Acta* 1862 (2021), 148330.
- [25]. Seravalli J, Ragsdale SW, Channeling of carbon monoxide during anaerobic carbon dioxide fixation, *Biochemistry* 39 (6) (2000) 1274–1277. [PubMed: 10684606]
- [26]. Chovancová E, Pavelka A, Beneš P, Strnad O, Brezovský J, Kozlíkov B, Gora A, Šustr V, Klva a M, Medek P, Biedermannová L, Sochor J, Damborský J, CAVER 3.0: a tool for the analysis of transport pathways in dynamic protein structures, *PLoS Comput. Biol* 8 (10) (2012), e1002708. [PubMed: 23093919]
- [27]. Dobbek H, Svetlitchnyi V, Liss J, Meyer O, Carbon monoxide induced decomposition of the active site [Ni 4Fe 5S] cluster of CO dehydrogenase, *J. Am. Chem. Soc* 126 (17) (2004) 5382–5387. [PubMed: 15113209]
- [28]. Domnik L, Merrouch M, Goetzl S, Jeoung J-H, Léger C, Dementin S, Fourmond V, Dobbek H, CODH-IV: a high-efficiency CO-scavenging CO dehydrogenase with resistance to O₂, *Angew. Chem. Int. Ed* 56 (48) (2017) 15466–15469.
- [29]. Doukov TI, Iverson TM, Seravalli J, Ragsdale SW, Drennan CL, A Ni-Fe-Cu center in a bifunctional carbon monoxide dehydrogenase/acetyl-CoA synthase, *Science* 298 (5593) (2002) 567–572. [PubMed: 12386327]
- [30]. Gong W, Hao B, Wei Z, Ferguson DJ, Tallant T, Krzycki JA, Chan MK, Structure of the $\alpha_2\epsilon_2$ Ni-dependent CO dehydrogenase component of the *Methanosarcina barkeri* acetyl-CoA decarbonylase/synthase complex, *Proc. Natl. Acad. Sci* 105 (28) (2008) 9558–9563. [PubMed: 18621675]
- [31]. Prangé T, Schiltz M, Pernot L, Colloc'h N, Longhi S, Bourguet W, Fourme R, Exploring hydrophobic sites in proteins with xenon or krypton, *Proteins* 30 (1) (1998) 61–73. [PubMed: 9443341]
- [32]. Schiltz M, Fourme R, Prangé T, Use of Noble gases xenon and krypton as heavy atoms in protein structure determination, *Methods Enzymol* 374 (2003) 83–119. [PubMed: 14696369]
- [33]. Mehio N, Dai S, Jiang D-E, Quantum mechanical basis for kinetic diameters of small gaseous molecules, *J. Phys. Chem. A* 118 (2014) 1150–1154. [PubMed: 24446751]
- [34]. Li L, Guo L, Zhang Z, Yang Q, Yang Y, Bao Z, Ren Q, Li J, A robust squarate-based metal–organic framework demonstrates record-high affinity and selectivity for Xenon over Krypton, *J. Am. Chem. Soc* 141 (2019) 9358–9364. [PubMed: 31091084]
- [35]. Darnault C, Volbeda A, Kim EJ, Legrand P, Vernède X, Lindahl PA, Fontecilla-Camps JC, Ni-Zn-[Fe4-S4] and Ni-Ni-[Fe4-S4] clusters in closed and open α subunits of acetyl-CoA synthase/carbon monoxide dehydrogenase, *Nat. Struct. Mol. Biol* 10 (2003) 271–279.
- [36]. Hadj-Saïd J, Pandelia M-E, Léger C, Fourmond V, Dementin S, The carbon monoxide dehydrogenase from *Desulfovibrio vulgaris*, *Biochim. Biophys. Acta* 1847 (2015) 1574–1583. [PubMed: 26255854]
- [37]. Wittenborn EC, Cohen SE, Merrouch M, Léger C, Fourmond V, Dementin S, Drennan CL, Structural insight into metallofactor maturation in carbon monoxide dehydrogenase, *J. Biol. Chem* 294 (2019) 13017–13026. [PubMed: 31296570]

- [38]. Rousset M, Dermoun Z, Chippaux M, Bélaich JP, Marker exchange mutagenesis of the hydN genes in *Desulfovibrio fructosovorans*, *Mol. Microbiol* 5 (7) (1991) 1735–1740. [PubMed: 1943706]
- [39]. Soltis SM, Stowell MHB, Wiener MC, Phillips GN, Rees DC, Successful flash-cooling of xenon-derivatized myoglobin crystals, *J. Appl. Crystallogr* 30 (2) (1997) 190–194.
- [40]. Kabsch W, XDS, *Acta Crystallogr. D Biol. Crystallogr* 66 (2) (2010) 125–132.
- [41]. McCoy AJ, Grosse-Kunstleve RW, Adams PD, Winn MD, Storoni LC, Read RJ, Phaser crystallographic software, *J. Appl. Crystallogr* 40 (4) (2007) 658–674. [PubMed: 19461840]
- [42]. Bunkoczi G, Read RJ, Improvement of molecular-replacement models with sculptor, *Acta Crystallogr. Sect. D* 67 (4) (2011) 303–312. [PubMed: 21460448]
- [43]. Schwarzenbacher R, Godzik A, Grzechnik SK, Jaroszewski L, The importance of alignment accuracy for molecular replacement, *Acta Crystallogr. Sect. D* 60 (7) (2004) 1229–1236. [PubMed: 15213384]
- [44]. Emsley P, Lohkamp B, Scott WG, Cowtan K, Features and development of coot, *Acta Crystallogr. Sect. D* 66 (4) (2010) 486–501. [PubMed: 20383002]
- [45]. Adams PD, Afonine PV, Bunkoczi G, Chen VB, Davis IW, Echols N, Headd JJ, Hung L-W, Kapral GJ, Grosse-Kunstleve RW, McCoy AJ, Moriarty NW, Oeffner R, Read RJ, Richardson DC, Richardson JS, Terwilliger TC, Zwart PH, PHENIX: a comprehensive Python-based system for macromolecular structure solution, *Acta Crystallogr. Sect. D* 66 (2) (2010) 213–221. [PubMed: 20124702]
- [46]. Painter J, Merritt EA, Optimal description of a protein structure in terms of multiple groups undergoing TLS motion, *Acta Crystallogr. Sect. D* 62 (4) (2006) 439–450. [PubMed: 16552146]
- [47]. Chen VB, Arendall III WB, Headd JJ, Keedy DA, Immormino RM, Kapral GJ, Murray LW, Richardson JS, Richardson DC, MolProbity: all-atom structure validation for macromolecular crystallography, *Acta Crystallogr. Sect. D* 66 (1) (2010) 12–21. [PubMed: 20057044]
- [48]. Schrodinger L, The PyMOL Molecular Graphics System, Schrödinger, LLC, 2020. Version 2.4.
- [49]. Morin A, Eisenbraun B, Key J, Sanschagrín PC, Timony MA, Ottaviano M, Sliz P, Collaboration gets the most out of software, *eLife* 2 (2013), e01456. [PubMed: 24040512]
- [50]. Stiebritz MT, Reiher M, Hydrogenases and oxygen, *Chem. Sci* 3 (6) (2012) 1739–1751.
- [51]. Abou Hamdan A, Liebgott P-P, Fourmond V, Gutiérrez-Sanz O, De Lacey AL, Infossi P, Rousset M, Dementin S, Léger C, Relation between anaerobic inactivation and oxygen tolerance in a large series of NiFe hydrogenase mutants, *Proc. Natl. Acad. Sci* 109 (49) (2012) 19916–19921. [PubMed: 23169623]
- [52]. Plume e N, Rüdiger O, Oughli AA, Williams R, Vivekananthan J, Pöller S, Schuhmann W, Lubitz W, A redox hydrogel protects hydrogenase from high-potential deactivation and oxygen damage, *Nat. Chem* 6 (9) (2014) 822–827. [PubMed: 25143219]
- [53]. Fourmond V, Stapf S, Li H, Buesen D, Birrell J, Rüdiger O, Lubitz W, Schuhmann W, Plumeré N, Léger C, Mechanism of protection of catalysts supported in redox hydrogel films, *J. Am. Chem. Soc* 137 (16) (2015) 5494–5505. [PubMed: 25835569]
- [54]. Dementin S, Leroux F, Cournac L, Lacey AL, Volbeda A, Léger C, Burlat B, Martínez N, Champ S, Martin L, Sanganas O, Haumann M, Fernández VM, Guigliarelli B, Fontecilla-Camps JC, Rousset M, Introduction of methionines in the gas channel makes [NiFe] hydrogenase aero-tolerant, *J. Am. Chem. Soc* 131 (29) (2009) 10156–10164. [PubMed: 19580279]
- [55]. Mohammadi M, Vashisth H, Pathways and thermodynamics of oxygen diffusion in [FeFe]-hydrogenase, *J. Phys. Chem. B* 121 (43) (2017) 10007–10017. [PubMed: 28975788]
- [56]. Kimura M, The neutral theory of molecular evolution: a review of recent evidence, *Jpn. J. Genet* 66 (4) (1991) 367–386. [PubMed: 1954033]
- [57]. Saitou N, Nei M, The neighbor-joining method: a new method for reconstructing phylogenetic trees, *Mol. Biol. Evol* 4 (4) (1987) 406–425. [PubMed: 3447015]

**Fig. 1.**

Comparison of hydrophobic channels in CODH complexes. All models were superposed on the CODH dimer and shown with the same orientation. Structures are *D. vulgaris* (PDB: 6B6V) [16], *R. rubrum* (PDB: 1JQK) [5], *C. hydrogenoformans* type II (PDB: 1SU6) [27], *C. hydrogenoformans* type IV (PDB: 6ELQ) [28], *M. thermoacetica* (PDB: 1MJG) [29], *M. barkeri* (PDB: 3CF4) [30], and *C. autoethanogenum* (PDB: 6YTT) [24]. Calculations were performed in CAVER [26] using a probe radius of 0.9 Å. The CODH dimer is colored in light and dark green, and ACS domains 1, 2, and 3 are colored in violet, navy, and light blue, respectively. Metalloclusters are shown as spheres with iron, sulfur, and nickel in orange, yellow, and green, respectively.

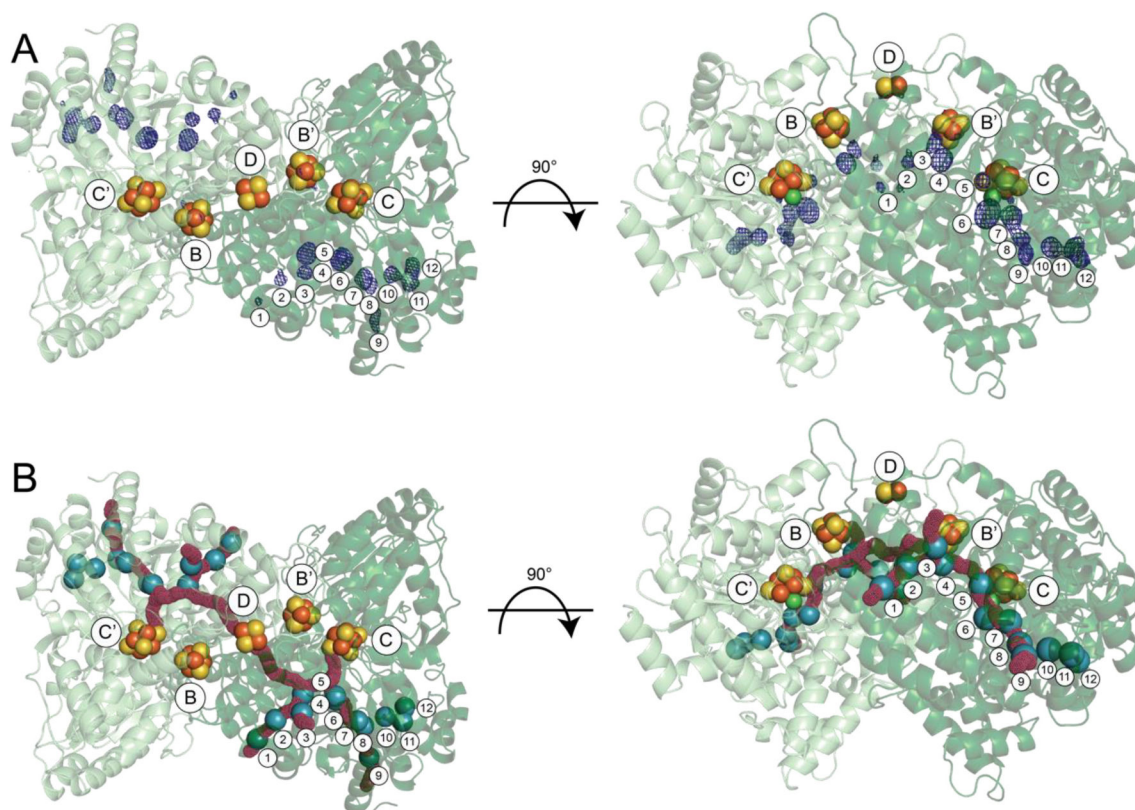


Fig. 2. Gas channels of *Dv*CODH as elucidated by xenon-bound CODH structures. (A) Anomalous difference map calculated from diffraction data collected at the xenon peak wavelength (2.0663 Å) contoured to 4σ and overlaid with *Dv*CODH structure. Although *Dv*CODH only has a monomer in the asymmetric unit, it is being displayed with its crystallographic symmetry mate to show the biologically relevant dimer. (B) Structure of xenon-bound *Dv*CODH with xenon as cyan spheres. CAVER predictions for the gas channel of *Dv*CODH are overlaid and colored in magenta. CODH and metalloclusters colored as in Fig. 1.

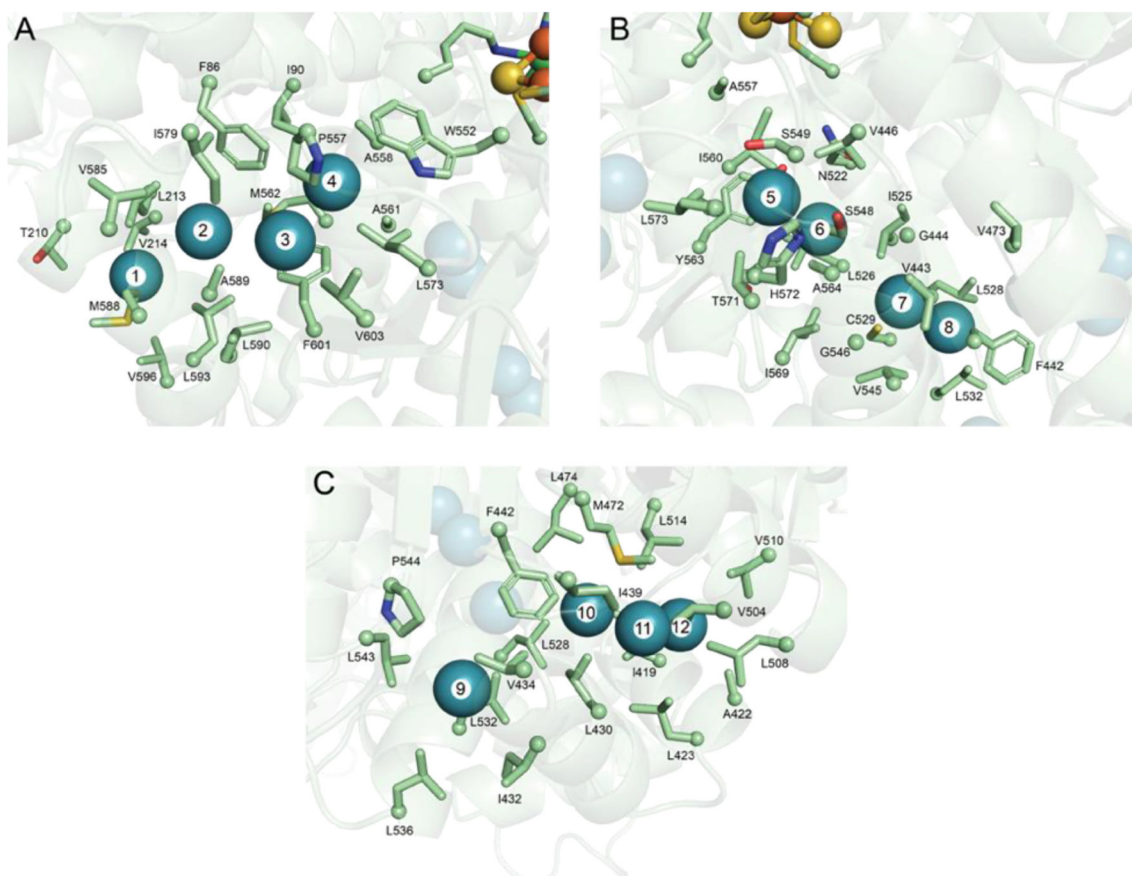


Fig. 3. Channel-forming residues in *Dv*CODH. Residues within 5 Å of xenon sites are shown as sticks with the alpha carbon shown as a ball. Colored as in Fig. 2. Xenon sites shown are: (A) xenon 1–4, (B) xenon 5–8, and (C) xenon 9–12.

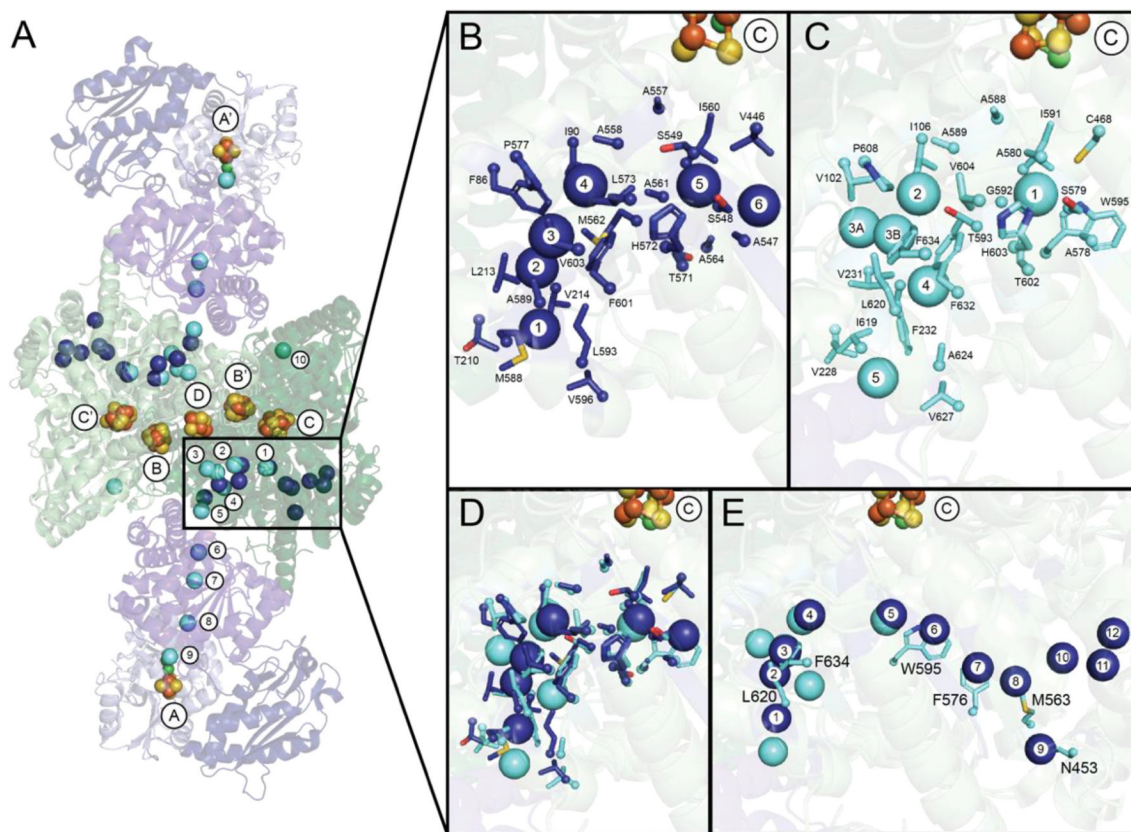


Fig. 4. Comparison of Xe sites in *D. vulgaris* and *M. thermoacetica* CODHs. (A) Overlay of xenon-bound *Dv*CODH and *Mc*CODH/ACS²². Xenon sites from *Mc*CODH/ACS are labeled 1–10. Colored as in Fig. 1, with xenon sites in *Dv*CODH colored in deep blue and xenon sites in *Mc*CODH/ACS colored in aquamarine. (B) Depiction of *Dv*CODH, with side chains in deep blue, showing channel-forming residues shared between *Dv*CODH and *Mc*CODH/ACS. (C) Depiction of *Mc*CODH/ACS, with side chains in aquamarine, showing channel-forming residues shared between *Dv*CODH and *Mc*CODH/ACS. (D) Overlay of shared channel-forming residues in *Dv*CODH and *Mc*CODH/ACS. (E) Channel-blocking residues in *Mc*CODH/ACS. Xenon sites from *Dv*CODH are labeled 1–12.

CLUSTAL W (1.83) multiple sequence alignment

```

D. vulgaris      MSSSKTI-----RSRSIWDDAHAMLEKAKAEGISTVWDRAAEQTPACKFCELGTTTCRNCIMGPCRIAN 63
R. rubrum       MTHHDC-----AHCSSDACATEMLNLAEANSIETAWHRYEKQPQCGFSGAGLCCRICLKGPCRIDP 62
C. hydrogenoformans II  MAKQNL-----KSTRAVQOQLDKAKREGIQTWDRYEAMKPOCGFGETLCCRRHCLQGPCRINP 60
C. hydrogenoformans IV  MDKSK-----LSVDPVIPNLRYKAREEGISTVFDRYEAQQPQCGFGLTLCRRHCVOGPCRIDP 59
M. thermoacetica  MPRFRDLSHNCRPSEAPRVMEPKNRDRTVDPVLEMLVKSDDKDVITAFDRFVAQQPQCKIYEGEICCFRCMAGPCRIKA 80
C. autoethanogenum  MEEKA-----KSIDQATLQLLDKAKQDGVETWDRKADMKVQCGFSGAGVCCRCNSMGPCRVSP 59

D. vulgaris      RKDGKMRLLGVCAGADADVIVARNFGRFAGGAAGHSDHGRDLIETLEAVAEKGAPGYTIRDAKLRRIAAELGVADAATRP 143
R. rubrum       FG-EGPKYVCGADRDTIVARHLVRMIAAGTAAHSEHGRHIALAMQHSIQGELHDYSIRDEAKLVIAIKTLGVAT-EGRG 140
C. hydrogenoformans II  FG-DEPKVIGCGATAEVI VARGLDRSIAAGAAGHSGHAKHLAHTLKKAVQGKAASYMIKDRTKLHSIAKRLGIDP-EGGK 138
C. hydrogenoformans IV  FG-EGPQAGICGATAEVI TARNLRQVTAGAAAHVVDHAYDVLVLEQIAQGT-ESYSIKDQEKLVQAVTLGIDT-ANKT 136
M. thermoacetica  TD-GPGSRGICGASAWTIVARNVGLMLTGAHAEHGNHIAHALVEMAEKGAPDYSVKDEAKLREKVCRRVIEV-EGKS 158
C. autoethanogenum  VPGKGVERICGATADVIVSRNFARMVAGTAAHSDHGRSIALSLYHTSK--DGDIVKVDENKLEKVAKSFNVET-EGRD 136

D. vulgaris      AHDVAADLVTCYNDFGSR--RNALA-FLARAPQVRRDLWQRLGTMTPRGVDREIAEMHRTMGMCDNDHTSLVHHAARTA 220
R. rubrum       LLAIVGDLAAITLGFDFONQDYDKPCAWLAASLTPRRVKRLGDLGLPHNIDASVAQTMRSRTHVGCADAPTNLLILGGLRVA 220
C. hydrogenoformans II  DEDIALEVAKAAALADFEK--DTPVLVWTVLPPSRVKVLSAHLIPAGIDHEIAEIMHRTSMGCDADACNLLLGLLRCS 216
C. hydrogenoformans IV  EQEIVEMECQIIRYDFANS-GATPMTYLVKANSPRELETWEKGLVLPNPDREIREALHQTMTMGMDADPVNLLIKTRIRLG 215
M. thermoacetica  VLELAQEVGEKALEDFRRLKGEGEATWLTMTINEGRKRFKTHNVVFPFIHASISELVNQAHMGMNDPVNLFVFAIRVA 238
C. autoethanogenum  IYDIAHDVAKEGLSNYKQ--LGEVT-LPPSLPEKRKELWRKLVYPRAVDREIAAVHSHTHIGCNADAAMIRMSMRCSS 213

D. vulgaris      LADGWGSMIGTELSLDFGTPRPROQTVNLGVLRKDAVNILVHGHNPVSEMI LAATREPAVRVAAQDAGA-ADINVG 299
R. rubrum       MAD-LDGSMLATELSDALFGTPQPVVSAANLGMKRGAVNIAVNGHNPMLSDIIDVAADL--RDEAIAAGAEGINIIG 297
C. hydrogenoformans II  LAD-LAGCYMGTDLADLFGTPAPVVTESNLGVLKADAVNVAVHGHNPVLSDIIVSVSKEM--ENEARAAGA-TGINLVG 292
C. hydrogenoformans IV  LVDGFAGLKLATDLQDIIIFGTPQPVVTEANLGVLEKEDYVNIIVHGHVPLSEKIVSEVSKEL--EENAKRAGA-RGINLAV 292
M. thermoacetica  LAD-YTGEHIATDFSDILFGTPQPVVSEANMGVLDPDQVNFVLHGHNPVLSSEIIVQAAREM--EGEAKRAGA-RGINLVG 314
C. autoethanogenum  LTDGWMGSFMGTEFSDIMFGTPHSIDTEANLGVLEKNSVNVVHLHGHEPLLSEMVVEAASDPVELLAKSVGA-DGINLVC 292

D. vulgaris      ICCTGNEMLMRQGI PMAGNHLMTELAIVTGAADAI VADYQCI MPSSLVQIAACYHTRFVTTSPKGRFTGATHVEVHPHNAQ 379
R. rubrum       ICCTGHEVMMRHGVP LANTYLSQELPILTGALAEAMVVDVQCIMPSLPIAECFTQIIITDDKHNKISGATHVPFDEHKAV 377
C. hydrogenoformans II  ICCTGNEVLMRHGIPACTHSVSQEMAMITGALDAMILDYQCIQPSVATIAECTGTVTITMEMSKITGATHVNFAEAAV 372
C. hydrogenoformans IV  ICCTGNEVLMRQGVPLATNFLAQELAITGAVDLMVVDVQCIMPSLAEIACVHTRLVITMPIVKIPGAEHVFPFTEAD 372
M. thermoacetica  ICCTGNEVLMRQGIPLVTSFASQELAICTGAIDAMCVDVQCIMPSISAVAECHYTRIIITADNAKIPGAYHIDYQTATAI 394
C. autoethanogenum  MCCTGNEVSMRHGIRIAGNFMOQELAVVTGAVDGLVDVQCIMPALAKLSKSYHTKFIITSPKHAITDSIYMEFDEENPL 372

D. vulgaris      ERCREIVMLAIDAYTRRDP--RVDIPSQPVSIMSGFSNEAILEALGG-----TPKPLIDAVVAGQIRGFGVIVG 447
R. rubrum       ETAKTIIRMAIAAFGRDPN--RVAIPAFKQKSI VGFSAEAVVAALAKV----NADDPLKPLIDNVNNGNIRGQIVLIFVG 450
C. hydrogenoformans II  ENAKQILRLAIDTFKRRK--PVEIPNKIKVAVGFS TEAINALSKL----NANDPLKPLIDNVNNGNIRGVCVIFAG 445
C. hydrogenoformans IV  EASQQIVRMAIESYQKRNP--KVYIPREKAVVAGFSVEAIVKALAKL----NPDDPLKPLIDNIVSGNILGVVAVTG 445
M. thermoacetica  ESAKTAIRMAIEAFKERKESNRPVYIPQIKNRVVAGWSLEALTKLLATQ----NAQNPVRVNLQAILDGLAGVALICG 469
C. autoethanogenum  DSAKKILKEALNFKNRDQS--KVMIPELKCKAILGYSVEEINKLKDKNVNTQIGPMQVTKPLADVLVSGVLRGAADVVG 450

D. vulgaris      CNNPKIRQDSANVTLTRELIRRDIMVLTGCVTTAAGKAGLLVPEAAS-KAGEGLAAVCRSLG-----VPPVLHMGS 518
R. rubrum       CNNTKVVQDSAYVDLAKSLAKRNLVLTATGCAAGAFKAGLMTSEATTQYAGEGLKGVLSAIGTAAGLGGPLPLVHMGS 530
C. hydrogenoformans II  CANNKVPQDNFTTIARKLLKQNVLVVATGCGAGALMRHGFMDPANVDELCDGLKAVLTAIGEANGLGGPLPPVHMGS 525
C. hydrogenoformans IV  CANNKVKHDFHIELVKEILLKNNVLVVTGCSAHALAKAGLMDPAAA-EWAGEGLRAVLTAGTANLGGPLPPVHMGS 524
M. thermoacetica  CANNKGFQDNHSLTVMKELLKNNVVFVATGCSAQAAGLGLLDPANVETVCGDGLKFLRLRLEGAGANIIEIGLPPVHMGS 549
C. autoethanogenum  CANNKVVQDSAHIETIKGLIKNDVIVVVTGCSAQAAGYGLLQKEAAEKYAGPGLATVCKLVD-----IPVVLHMGS 522

D. vulgaris      CVDNSRILQCALLATLGVDISDLPV GASSPEWYSEKAAAIAMYAVASGIPHTLGLPPNIGLSENVTAMALHGLQDVVG 598
R. rubrum       CVDNSRAVALATALANKLGVLDLPLVASAPECMSEKALAI GSWAVTIGLPTHVGSVPPVIGSQIVTKLVETAARDLVG 610
C. hydrogenoformans II  CVDNSRAVALVAALANRLGVLDLPLVVASAAEAMHEKVAIGTAVTIGLPTHIGVLPPTIGSLPVPTILTSSVKIDITG 605
C. hydrogenoformans IV  CVDNSRIGDLVIAVANLYKVS PKDLPV IASAPEYQHEKALSIGTWAVAMGIMTHLGVVPPVVGSKVPTILTQDAEALIG 604
M. thermoacetica  CVDNSRAVDLLMAMANDLGVDPKVPVVASAPEAMSGKAAAI GVTWVSLGVPTHTGTPPVEGSDLIYSILTQASDVVG 629
C. autoethanogenum  CVDISRILLDVGVRVANLLGVDMSDLVAVGAPVEMSEKVAIGTYVVTSGIDTWLGVAPPVVTGPEVVDILNKMKEDVVG 602

D. vulgaris      AAFMVPEPDKAADMLEAHIVARRARLGLTS----- 629
R. rubrum       GYFIVDTPKSAGDKLYAIIQERRAGLGL----- 639
C. hydrogenoformans II  GYFIVELDPETAADKLLAAINERRAGLGLPW----- 636
C. hydrogenoformans IV  GKFYVETDPYKAAAGIIEHIAKAKRALLNL----- 633
M. thermoacetica  GYFIFEMDPQVAARKILDALRYTWKLVGHVEAERYETKLCQGY 674
C. autoethanogenum  AKFFIETDPHKAIVEIVNRMNEKRRKLGII----- 631

```

Fig. 5. Sequence alignment of CODHs. Channel-forming residues from *Dv*CODH are colored in green. At the equivalent position in all other CODHs, residues with the same identity also are colored in green, those with similar biochemical properties are colored in yellow, and those with different biochemical properties are colored in orange. Residues clashing with xenon atoms bound to *Dv*CODH are shown in magenta.

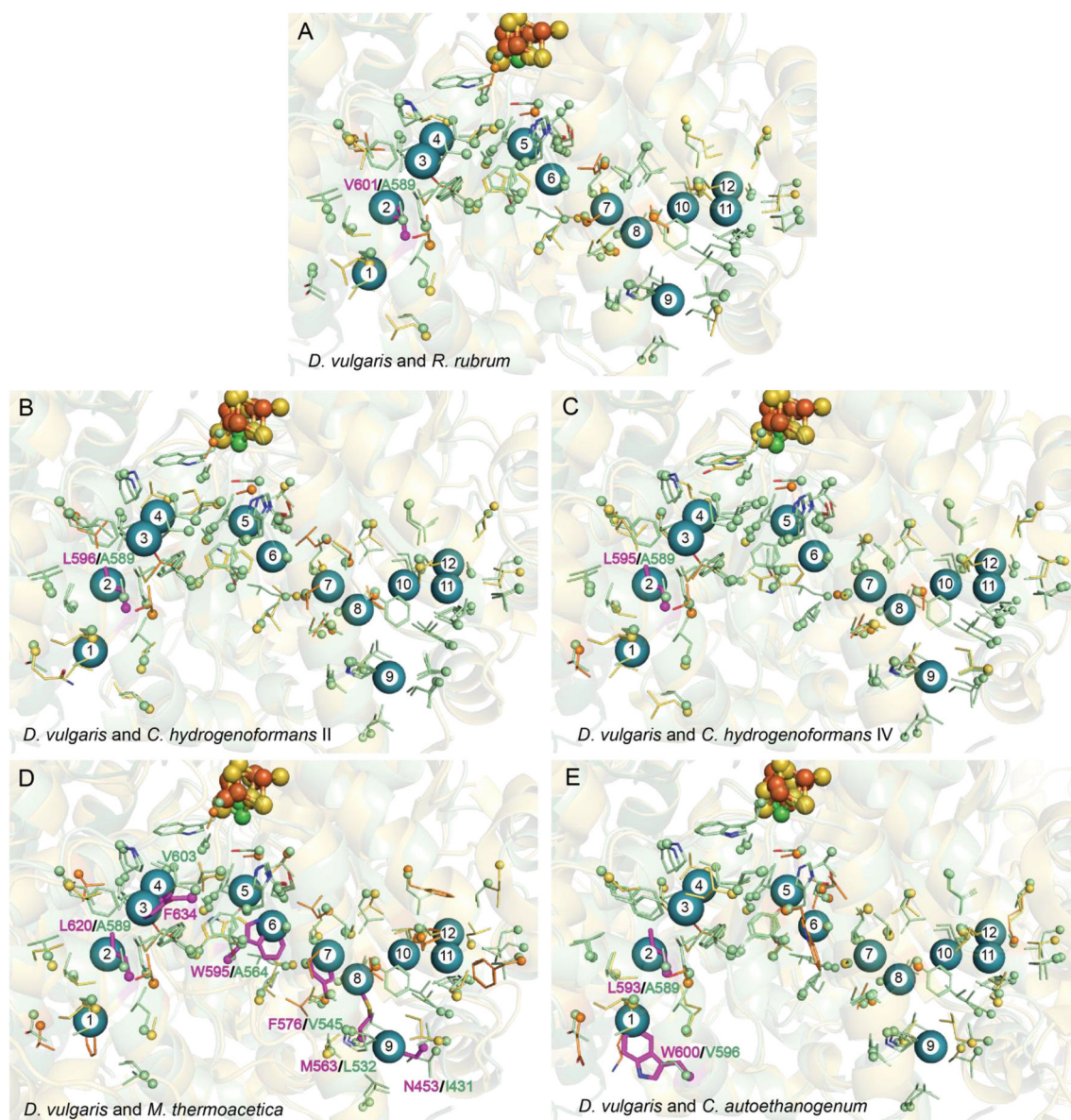


Fig. 6. Structural comparison of *Dv*CODH gas channel-forming residues with other CODHs aligned. (A) *R. rubrum* (PDB: 1JQK) [5]. (B) *C. hydrogenoformans* type II (PDB: 1SU6) [27]. (C) *C. hydrogenoformans* type IV (PDB: 6ELQ) [28]. (D) *M. thermoacetica* (PDB: 2Z8Y) [22]. (E) *C. autoethanogenum* (PDB: 6YTT) [24]. *Dv*CODH shown in green. At the equivalent position in all other CODHs, residues with the same identity are colored in green, with similar biochemical properties are colored in yellow, and with different biochemical properties are colored in orange. All xenon atoms shown are bound to *Dv*CODH and depicted in cyan. Residues clashing with xenon are shown in magenta. Metalloclusters colored as in Fig. 1. See SI Figs. S4–S5 for versions of Figs. 5–6 that have more residue identification information.

Table 1

Crystallographic data collection and refinement statistics.

	Native PDB CODE: 7TSJ	Xe peak [^]
Data collection Space group	C2	C2
Cell dimensions		
<i>a</i> , <i>b</i> , <i>c</i> (Å)	113.9, 100.9, 65.4	113.9, 100.9, 65.4
α , β , γ (°)	90.0, 124.9, 90.0	90.0, 124.9, 90.0
Resolution (Å) [*]	46.75–2.10 (2.17–2.10)	46.84–3.08 (3.19–3.08)
<i>R</i> _{sym} (%) [*]	6.2 (51.7)	10.1 (72.6)
CC _{1/2} [*]	99.7 (86.5)	99.7 (65.2)
$\langle I / \sigma I \rangle$ [*]	12.6 (2.6)	9.3 (1.7)
Completeness (%) [*]	97.7 (98.2)	97.5 (97.2)
Redundancy [*]	3.9 (3.5)	3.4 (3.1)
No. unique reflections [*]	34,865 (3500)	21,695 (2151)
Refinement Resolution (Å)	46.73–2.10	
<i>R</i> _{work} / <i>R</i> _{free} [†]	0.169/0.210	
No. atoms		
Protein	4621	
B-cluster	8	
C-cluster	9	
D-cluster	2 [‡]	
Xenon	12	
Water	74	
<i>B</i> -factors (Å ²)		
Protein	50.3	
B-cluster	38.4	
C-cluster	50.6	
D-cluster	45.2	
Xenon	52.9	
Water	48.0	
R.m.s. deviations		
Bond lengths (Å)	0.007	
Bond angles (°)	0.82	
Rotamer outliers (%)	1.88	
Ramachandran (%)		
Favored	96.6	
Allowed	3.1	
Disfavored	0.3	
Residues (of 629)		
Chain A	8–628	

* Values in parentheses are for the highest-resolution shell.

† 5.22% of reflections were set aside for test set.

‡ For this structure, the D-cluster was refined as one iron with one sulfur, given the presence of monomer in the ASU.

^ Friedel's pairs were not merged.

Author Manuscript

Author Manuscript

Author Manuscript

Author Manuscript